

Resonance scattering by auroral N_2^+ : steady state theory and observations from Svalbard

O. Jokiahho¹, B. S. Lanchester¹, and N. Ivchenko²

¹School of Physics and Astronomy, University of Southampton, UK

²Space and Plasma Physics, School of Electrical Engineering, KTH, Stockholm, Sweden

Received: 11 May 2009 – Revised: 10 August 2009 – Accepted: 19 August 2009 – Published: 4 September 2009

Abstract. Studies of auroral energy input at high latitudes often depend on observations of emissions from the first negative band of ionised nitrogen. However, these emissions are affected by solar resonance scattering, which makes photometric and spectrographic measurements difficult to interpret. This work is a statistical study from Longyearbyen, Svalbard, Norway, during the solar minimum between January and March 2007, providing a good coverage in shadow height position and precipitation conditions. The High Throughput Imaging Echelle Spectrograph (HiTIES) measured three bands of N_2^+ 1N (0,1), (1,2) and (2,3), and one N_2 2P band (0,3) in the magnetic zenith. The brightness ratios of the N_2^+ bands are compared with a theoretical treatment with excellent results. Balance equations for all important vibrational levels of the three lowest electronic states of the N_2^+ molecule are solved for steady-state, and the results combined with ion chemistry modelling. Brightnesses of the (0,1), (1,2) and (2,3) bands of N_2^+ 1N are calculated for a range of auroral electron energies, and different values of shadow heights. It is shown that in sunlit aurora, the brightness of the (0,1) band is enhanced, with the scattered contribution increasing with decreasing energy of precipitation (10-fold enhancements for energies of 100 eV). The higher vibrational bands are enhanced even more significantly. In sunlit aurora the observed 1N (1,2)/(0,1) and (2,3)/(0,1) ratios increase as a function of decreasing precipitation energy, as predicted by theory. In non-sunlit aurora the N_2^+ species have a constant proportionality to neutral N_2 . The ratio of 2P(0,3)/1N(0,1) in the morning hours shows a pronounced decrease, indicating enhancement of N_2^+ 1N emission. Finally we study the relationship of all emissions and their ratios to rotational temperatures. A clear effect is observed on rotational development of the bands. It is possible that

greatly enhanced rotational temperatures may be a signature of ion upflows.

Keywords. Atmospheric composition and structure (Airglow and aurora; Transmission and scattering of radiation) – Ionosphere (Auroral ionosphere)

1 Introduction

Emissions from the nitrogen molecule are of great importance in auroral studies. Firstly, they are used as diagnostics for the total energy flux, since the brightness of these emissions is only weakly dependent on the characteristic energy. Secondly, spectral measurements of N_2^+ bands can be used to determine the rotational temperature. Thermal equilibrium of atmospheric constituents allows us to assume that the rotational temperature is a measure of the atmospheric neutral temperature of the emitting species. Hence it is possible to infer the height of the auroral excitation, from which is estimated the characteristic energy.

The auroral N_2^+ 1N band system in the UV (from $B^2\Sigma_u^+$ to $X^2\Sigma_g^+$) is caused by electron impact ionisation and excitation of the N_2 molecules. However, when N_2^+ ions are illuminated by sunlight above the shadow height at high latitudes, the 1N band system will scatter and fluoresce, enhancing brightness and leading to an increase in vibrational and rotational temperatures. Different bands are affected in different ways, so that the ratios of emissions will vary with shadow height. Therefore during sunlit or partially sunlit conditions the measured values of emission intensities (and rotational temperatures) will lead to uncertainties in the characteristic electron energy and energy flux. The average energy from rotational spectra can be underestimated due to the contribution from highly developed sunlit spectra. Similarly, the flux can be overestimated in a simple photometric measurement when the brightness is increased due to the scattered contribution.



Correspondence to: O. Jokiahho
(oj@soton.ac.uk)

Abnormally bright N_2^+ was first observed by Störmer (1955) in the early 1910s. Triangulation indicated the rays were located above 1000 km. The observation that sunlit rays occur between a year before and three years after sunspot maximum can be related to the significant increase of the exospheric temperature from 1000 K to 2000 K, and expansion of the upper atmosphere at the maximum of solar UV activity. Sunlit measurements have usually been recorded away from the magnetic zenith (Broadfoot, 1967; Vallance Jones and Hunten, 1960). The latter reported unusually high rotational and vibrational temperatures of 2200 K during the 1958 solar maximum. An historical account of resonance scattering from N_2^+ can be found in Hunten (2003).

The theoretical foundation for resonance scattering of N_2^+ ions was set up by Bates (1949). Broadfoot (1967) later demonstrated how the vibrational distribution is strongly affected by resonance scattering and highlighted the method of using the relative intensities and populations of excited states to give an estimate of the two excitation sources. Ionisation from photoionisation is indistinguishable from electron impact because the ionisation efficiency is very similar; the former dominates in twilight and daytime non-auroral conditions, and the latter in sunlit and non-sunlit aurora. More enhanced vibrational development in twilight spectra in comparison to sunlit aurora is also reported. Broadfoot modelled steady state populations for all important vibrational levels of the N_2^+ $X^2\Sigma_g^+$, $A^2\Pi_u$ and $B^2\Sigma_u^+$ as a function of ion lifetime and reported a 40% contribution of resonance scattering to N_2^+ 1N bands.

Degen (1981) used new cross sections in the model of Broadfoot (1967) which raises ion lifetimes in sunlit aurora by an order of magnitude. He found that resonance scattering contributed 56% of the 1N intensities, pointing out the relative population increase with increasing vibrational level v' . Degen also introduced low energy electron induced fluorescence analogous to solar induced fluorescence to explain vibrational enhancement of the 1N band in the great type-A aurora of 1958 in non-sunlit conditions. The model was revisited by Degen (1987) when he modified the N_2^+ 1N (0,0) rotational band structure by varying the ion life time and rotational temperature. The results were compared favourably with sunlit auroral data of Hunten et al. (1959).

The characteristic intensity minimum just below the shadow height of aurora that is partly sunlit has long been observed with scanning photometers. N_2^+ 1N (0,1) height profiles of volume emission rate were studied by Lanchester et al. (1987) over Svalbard. In the morning sector these profiles had the characteristic double hump feature due to the contribution from resonance scattering. In that work the resonance scattering contribution was subtracted in order to estimate the energy of precipitation from brightness ratios.

Romick et al. (1999) provided the first space borne spectrographic observation of auroral emissions above 600 km from the N_2^+ 1N and M band systems, reporting emissions

up to 900 km over the northern polar cap close to magnetic noon. No other significant optical emissions were detected above 450 km suggesting the source was resonance scattering of the N_2^+ ions in the presence of ion upflows. They measured up to a 40% contribution in the 1N band system intensity above the shadow height with $K_p=3$ and a 4% contribution with $K_p=1$.

Remick et al. (2001) conducted simultaneous observations of N_2^+ 1N (0,1) with N_2^+ M (0,0) at Poker Flat, Alaska over two seasons between 1995 and 1997. Emission rates of the two bands should be in strict proportion over a wide energy range, which was not found. The lack of proportionality was explained by the increase in the 1N band system intensity by resonance scattering. They concluded that there exists a short duration episodic acceleration mechanism in the presence of auroral arcs that lifts ions into the sunlit region of the ionosphere.

The present work sets out to quantify the effect of sunlit conditions on zenith measurements under a steady state. It follows work of Jokiahho et al. (2008), which used the N_2^+ 1N (0,2) band to determine the rotational temperature and thus estimate the energy of precipitation, in conjunction with the EISCAT Svalbard Radar. In the present work, we make a statistical study of spectral measurements of three N_2^+ 1N bands (1,0), (1,2) and (2,3), and one N_2 2P band (0,3). We investigate the brightness ratios of the N_2^+ bands and their ratio to the N_2 band, since in resonance scattered auroral events the relationship between them can be used as an indicator of the scattered contribution. We also study the relationship of all emissions and their ratios to rotational temperatures. The theoretical basis of the study is provided in Sect. 3, giving a method of quantifying the scattering enhancement and the effect on rotational temperatures, as well as the possible effect of ion upflows.

2 Experimental details and analysis

We report a statistical study of night-time, twilight and daytime (cusp) aurora at the solar minimum from the magnetic zenith between 17 January and 14 March 2007 at Adventdalen in Longyearbyen, Svalbard (78° N, 15° E). The experiment used the High Throughput Imaging Echelle Spectrograph (HiTIES) (Chakrabarti et al., 2001) equipped with a water cooled Andor iXon EMCCD camera and a five panel interference filter mosaic seen in Fig. 1, which was designed to measure the effect of resonance scattering of solar photons in aurora by N_2^+ molecules. Height integrated spectral profiles were obtained for the study with a temporal resolution of 10–30 s.

Spectral bands of interest are the N_2^+ 1N and N_2 2P band systems that both lie in the near UV region. The most suitable bands were selected from the overlapping spectral orders of the echelle that could be transmitted simultaneously with sufficient brightness and without excess contamination.

Table 1. The spectral properties of the five panels of the interference filter mosaic.

	Wavelengths	Emissions
Panel 1	402.9–406.2 nm	N ₂ 2P (0,3), HgI
Panel 2	481.0–487.2 nm	Hβ
Panel 3	421.6–428.3 nm	N ₂ ⁺ 1N (0,1) and (1,2)
Panel 4	418.6–420.8 nm	N ₂ ⁺ 1N (2,3)
Panel 5	647.5–661.2 nm	Hα

These spectral bands are given in Table 1. The mosaic selects orders containing the bands of: N₂⁺ 1N (0,1) at 427.8 nm, (1,2) at 423.6 nm, (2,3) at 419.9 nm and N₂ 2P (0,3) at 405.8 nm. Some atomic lines are also seen, namely N⁺ at 423.7 nm, O⁺ doublet centred at 419 nm, contaminant mercury HgI at 404.7 nm, all of which are outside the bands of interest. The Hα and Hβ lines are excited in proton aurora (Galand et al., 2004) which is one of the science objectives of the SIF instrument (Lanchester et al., 2003). In this study of resonance scattering we do not analyse the hydrogen emissions.

Wavelength calibration of the instrument was performed using data from a period with a bright aurora in the field of view. The observed position of identifiable spectral features were related to their tabulated wavelengths. The focusing was optimised for best wavelength resolution in the R-branch rotational lines of the N₂⁺ 1N (0,1). A flat lamp was used for intensity calibration of the data.

A sketch of the rectangular interference filter is represented in Fig. 1. The vertical axis corresponds to wavelength and the horizontal axis translates into field of view of 8°. The three N₂⁺ 1N bands are recorded from 2° centred at the magnetic zenith. The adjacent N₂ 2P and proton line filters are centred 2° off magnetic zenith. Figure 2 shows a typical auroral spectra used in this study. The prominent emissions in order of increasing wavelength are HgI, N₂ 2P (0,3), N₂⁺ 1N (2,3), (1,2) and (0,1). The presence of HgI indicates reflection of artificial lighting from the cloud cover above and is overlaid on auroral data for comparison. The wavelength intervals used for deriving the brightness of the bands are highlighted in colour.

The total band intensities were calculated by integrating the observed spectral brightnesses over wavelength intervals of 427.9–424.5 nm for the N₂⁺ 1N (0,1), 423.8–422.3 nm for the N₂⁺ 1N (1,2), 419.5–420.0 nm for the N₂⁺ 1N (2,3) and 405.6–406.0 nm for the N₂ 2P (0,3). The background levels are different for each of the bands and these were measured by taking an average of the spectral brightness outside the integrated region. The background brightness of N₂⁺ 1N (0,1) and (1,2) was estimated from the longer wavelength side of the N₂⁺ 1N (0,1) band head. The background for N₂⁺ 1N (2,3) is determined from the region 418.5–419.5 nm. The atomic oxygen lines are very weak and allow a reason-

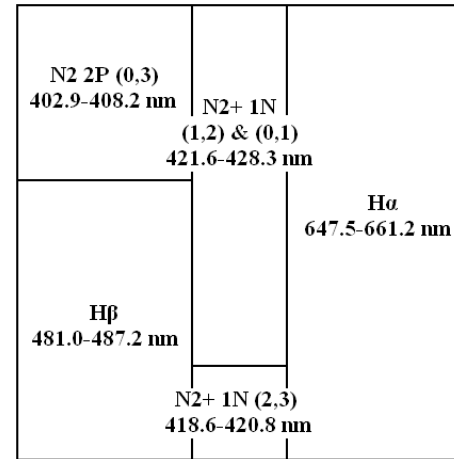


Fig. 1. The HiTIES spectrograph is equipped with a 50×50 mm square mosaic consisting of five interference filters. The 8° field of view is on the horizontal axis and wavelength on the vertical axis.

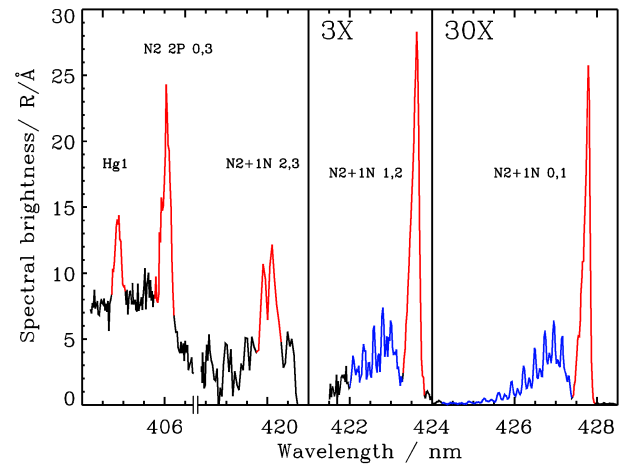


Fig. 2. Sample data from the HiTIES spectrograph using a 5-band mosaic filter (excluding the Hα and Hβ lines). The highlighted spectral features here correspond in increasing wavelength to HgI (red) overlaid from cloudy data, N₂ 2P (0,3) (red), N₂⁺ 1N (2,3) (red), N₂⁺ 1N R of (1,2) (blue) P of (1,2) (red) and N₂⁺ 1N R of (0,1) (blue) and P of (0,1) (red).

able noise level to be measured. The longer wavelength side of the band head cannot be used as the instrument response falls off rapidly due to optical vignetting at the edge of the mosaic. The background for N₂ 2P (0,3) is measured between the HgI and the N₂ 2P (0,3) features.

Low brightness and increased experimental uncertainty is associated with decreased instrument response in the UV. Spectral features other than N₂⁺ 1NG (0,1) and (1,2) are subject to greater uncertainties so that the band structure is difficult to resolve. The N₂ 2P (0,3) and N₂⁺ 1NG (2,3) band

Table 2. Franck-Condon factors from Gilmore et al. (1992)^a and Lofthus et al. (1977)^b.

v', v'''	0,0	1,0	2,0
^a N ₂ X-N ₂ ⁺ B	8.83-1	1.14-1	2.31-3
^b N ₂ X-N ₂ ⁺ B	8.864-1	1.112-1	2.335-3

typically account for only a few percent at most of the N₂⁺ 1NG (0,1) intensity and are situated further into the UV region. N₂ 2P is a Π-Π triplet transition and forms one distinct band head which makes it easier to detect. The low flat lamp spectral brightness in the near UV also added some uncertainty in the measurements.

The rotational temperatures of the N₂⁺ were derived using the χ^2 statistic (Jokiahho et al., 2008) with the N₂⁺ 1NG (0,1) band profiles. The standard deviation in height integrated rotational temperatures depends on the excitation conditions. It also depends on the temperature itself as the intensity distribution is more dynamic at lower temperatures than at higher temperatures. The overlapping of N₂⁺ bands also needs to be considered at high rotational temperatures. The rotational band profiles were acquired by subtracting the correct level of background output from the statistical process.

3 Theoretical approach

The N₂⁺ 1N band system results from simultaneous ionisation and excitation of the N₂X state via electron collisions to the N₂⁺ B state followed by radiative de-excitation to the ion ground state. During non-sunlit conditions, the emission is proportional to the ionisation rate.

The N₂⁺ ion ground state is an efficient scatterer of solar photons. The molecules in the X state that are sunlit above the shadow height are excited to the N₂⁺ A and N₂⁺ B states through a resonance process, resulting in increased brightness in the Meinel and the 1N band systems respectively. Following Broadfoot (1967) and Degen (1981), we consider excitation and de-excitation of vibrational levels of N₂⁺ X, A, B states to determine the brightness of the 1N bands in sunlit aurora in different conditions.

The time dependent population of the vibrational levels in the X, A and B states is described by

$$\frac{dn}{dt} = \text{Production-Losses} \quad (1)$$

Sources of the N₂⁺ X state include direct excitation from the N₂ X state via electron impact and radiative transitions from the N₂⁺ A and B states. Sources for the A and B states also include direct excitation via electron impact from the N₂ X state. Another source for the excited N₂⁺ A and B states is the resonance absorption of solar photons from the N₂⁺ X ground state vibrational levels.

Table 3. Einstein coefficients from Gilmore et al. (1992)^a, Lofthus et al. (1977)^b, and Vallance Jones (1974)^c.

v', v''	0,1	1,2	2,3
^a A _{v'v''}	3.71+6	4.28+6	3.47+6
^b A _{v'v''}	3.48+6	3.87+6	3.03+6
^c A _{v'v''}	3.35+6	3.81+6	3.13+6
^a ∑ _{v''} A _{v'v''}	16.05+6	16.11+6	15.91+6
^b ∑ _{v''} A _{v'v''}	14.05+6	13.82+6	13.34+6
^c ∑ _{v''} A _{v'v''}	15.15+6	15.97+6	16.64+6

Loss factors for the N₂⁺ X state are resonance absorption of solar photons into the higher states and for the N₂⁺ A and B states the loss factors are prompt emissions. All states are affected by ion chemical losses through collisions. This ion life time depends on the relevant reaction rate and is height dependent.

An updated ion chemistry model (Palmer, 1995) is used that treats N₂⁺ as a single species and produces time dependent height profiles of the N₂ molecular concentration using the relevant electron impact excitation cross sections and input primary electron spectra. We assume only local production of N₂⁺. We also do not take into account ionisation by photoelectrons or excitation from N₂⁺ X to A and B by soft electrons (Degen, 1981).

3.1 Direct excitation

The production of ions in different vibrational levels v' of N₂⁺ X, A, B states is given by

$$\eta_{v''' \rightarrow v'', v'}^d = \int_E n_{v'''} f(E) \sigma^e(E) \varepsilon(X, B, A) q_{(v''' \rightarrow v'', v')} dE \quad (2)$$

where $\eta_{(v''' \rightarrow v'', v')}^d$ is the production rate of N₂⁺ into level v' or v'' from a particular v''' , $n_{v'''}$ is the concentration of ground state N₂ molecules, $f(E)$ is the incident electron differential energy flux, $\sigma^e(E)$ is the total electron ionising excitation cross section of the N₂ ground state to all three ion states and $q_{v''' \rightarrow v'', v'}$ is the Franck-Condon factor for each level. We use $\varepsilon(X, A, B)$ to describe the ionisation efficiency, given by the branching ratios between the production rate of X, A and B states, which are 0.50, 0.39, 0.11, respectively (Rees, 1989). The standard prime convention is used to describe vibrational levels. v''' relates to the N₂ X vibrational levels, v'' relates to the N₂⁺ X vibrational levels and v' relates to the excited N₂⁺ A, B vibrational levels. Franck-Condon factors are taken from Gilmore et al. (1992), listed in Table 2 for three N₂⁺ B vibrational levels from the $v'''=0$ vibrational level of N₂ X. Franck-Condon factors from Lofthus et al. (1977) are also listed for reference. At vibrational temperatures above 1000 K, higher vibrational levels need to be considered.

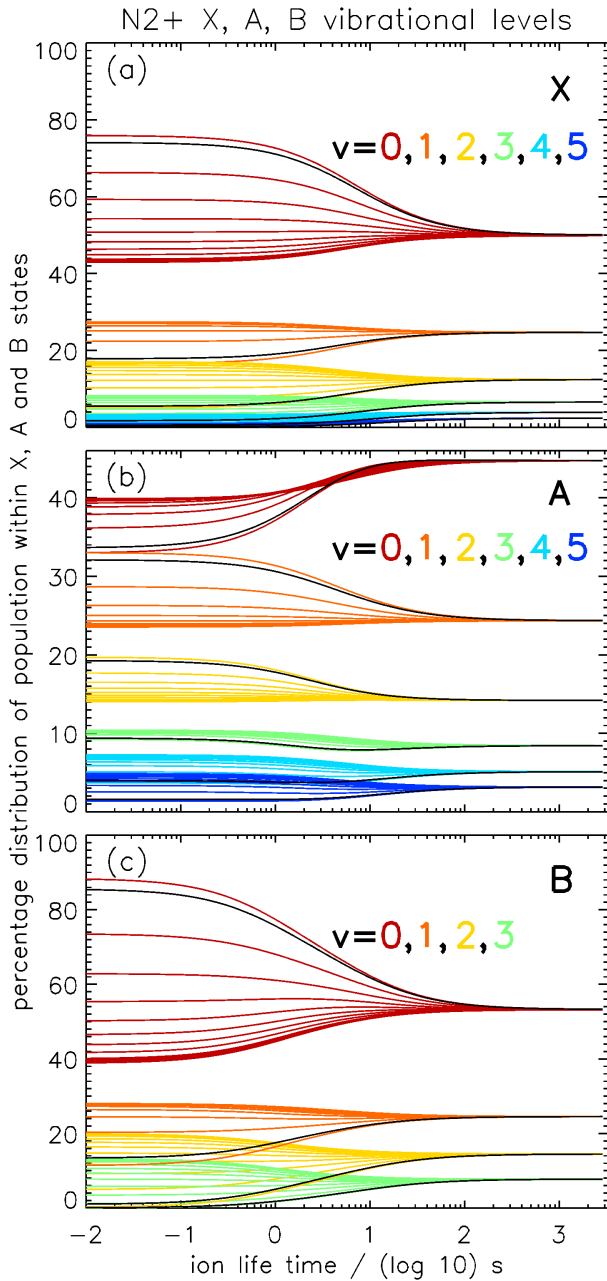


Fig. 3. Vibrational distribution of ion states as a function of ion chemical lifetime, for $T_{\text{vib}}=100-10\,000$ K in steps of 1000 K ($T_{\text{vib}}=1000$ is highlighted in black and is very close to $T_{\text{vib}}=100$): (a) $v''=0-5$ for N₂⁺ X, (b) $v''=0-5$ for N₂⁺ A and (c) $v''=0-3$ for N₂⁺ B.

If the total ion production rate is known, e.g. from the ion chemistry model, Eq. (2) can be rewritten as

$$\eta_{(v'' \rightarrow v'', v')}^d = \varepsilon(X, B, A) q_{(v'' \rightarrow v'', v')} \eta_{N_2^+}^d \quad (3)$$

where $\eta_{N_2^+}^d$ is the total production rate of N₂⁺.

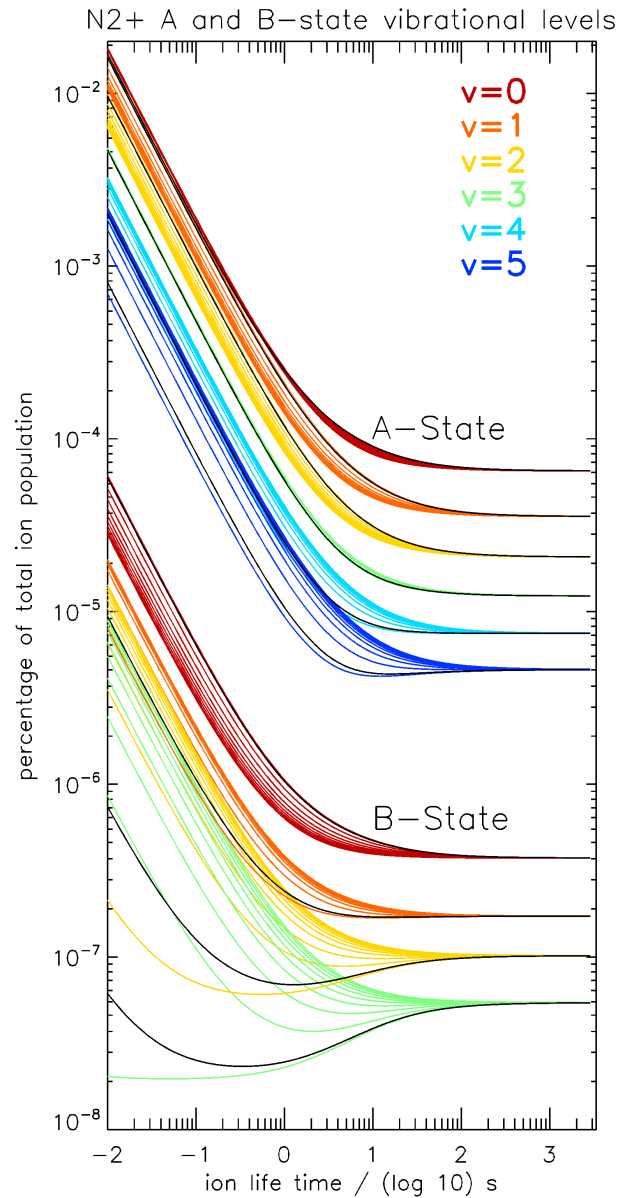


Fig. 4. Vibrational distribution of ion states in levels $v'=0-5$ of the N₂⁺ A state and vibrational levels $v'=0-3$ of the N₂⁺ B state with respect to the total population in all X, A and B states as a function of ion chemical lifetime. $T_{\text{vib}}=100-10\,000$ K in steps of 1000 K with $T_{\text{vib}}=1000$ highlighted in black.

3.2 Resonance absorption of solar photons

When N₂⁺ molecules in the X-state are sunlit, resonance absorption of solar photons results in excitation rate η^s into the A and B ion states.

$$\eta_{v'' \rightarrow v'}^s = \pi F_{v'' \rightarrow v'} f_{v'' \rightarrow v'} \frac{\pi e^2}{m_e c} \frac{1}{4\pi \epsilon_0} \frac{\lambda^2}{c} n_{v''} \quad (4)$$

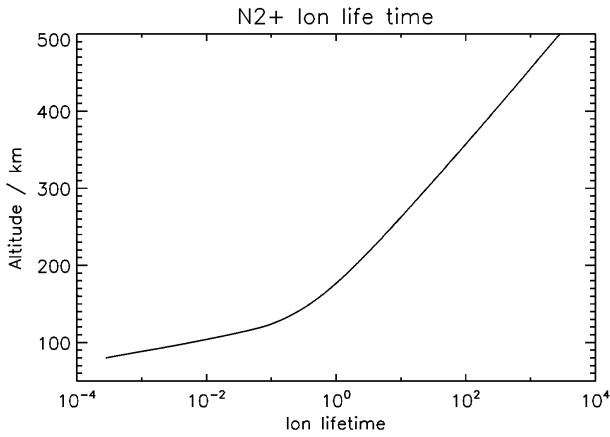


Fig. 5. Ion lifetime derived from the ion chemistry model using the MSIS atmospheric thermal model for a typical atmosphere at 07:00 UT in January over Svalbard with A_p index of 7 and solar radio flux f107av of 77.

where $\pi F_{v'' \rightarrow v'}$ is the solar flux per unit wavelength [photons $\text{m}^{-2} \text{s}^{-1} \text{m}^{-1}$], $f_{v'' \rightarrow v'}$ is the absorption oscillator strength, $\frac{\pi e^2}{m_e c} \frac{1}{4\pi\epsilon_0} \frac{\lambda^2}{c}$ [m^3] is the photon absorption cross section multiplied by the line width. The factor $\frac{\lambda^2}{c}$ is for conversion from spectral flux per unit frequency to flux per unit wavelength. $n_{v''}$ is the concentration of N₂⁺ in the X state vibrational level v'' .

3.3 Emission processes

Radiative transitions to the N₂⁺ X state are loss processes for the A and B states. The emission rate in a particular band is given by the Einstein coefficient as follows

$$\eta_{v' \rightarrow v''} = A_{v' \rightarrow v''} n_{v'} \quad (5)$$

Total radiative loss for a given v' state is

$$\eta_{v'} = \sum_{v''} A_{v' \rightarrow v''} n_{v'} \quad (6)$$

with the emission in each particular band given by the branching ratio

$$b_{v' \rightarrow v''} = \frac{\eta_{v' \rightarrow v''}}{\eta_{v'}} = \frac{A_{v' \rightarrow v''}}{\sum_{v''} A_{v' \rightarrow v''}} \quad (7)$$

Einstein coefficients are available from several sources. We have used the most recent values of Gilmore et al. (1992). These are given in Table 3 along with those from Lofthus et al. (1977) and Vallance Jones (1974) for comparison.

3.4 Steady state solutions

Equation (1) can be solved in a time dependent manner, which is outside the scope of this paper. Setting $\frac{dn}{dt}$ to zero we perform calculations for steady state conditions for each

vibrational level of the N₂⁺ A, B and X states, as described in Eqs. (11), (12) and (13), respectively, where the gain and loss terms are as previously described. These balance equations can be regrouped as a linear system of equations in the form of

$$\sum_j \mathbf{M}_{ij} n_j = \eta_i^d \quad (8)$$

where \mathbf{M}_{ij} is the matrix characterising production and loss processes, n_j is the concentration of each particular electronic-vibration level and η_i^d is the direct production rate of each electronic-vibration state due to auroral precipitation. This equation can be solved by matrix inversion

$$n_j = \mathbf{M}_{ij}^{-1} \eta_i^d \quad (9)$$

to provide equilibrium concentrations of all considered electronic-vibration states. Absolute values of the densities of the states are proportional to the total ionisation rate as the system is considered linear, while the ratios of densities are constant and are given by the molecular constants, solar flux and ion lifetime.

The steady state equilibrium density distribution within the N₂⁺ X, A and B states are plotted in Fig. 3a, b and c as a function of ion lifetime assuming the ionosphere is sunlit. The percentage population of N₂⁺ in the X state is plotted for vibrational levels $v''=0-5$, in the A state for vibrational levels $v'=0-5$ and in the B state for vibrational levels $v'=0-3$. At high altitudes the long ion lifetime allows more scattering to take place and is therefore dominated by resonance absorption, whereas at low altitudes the short ion lifetime enforces a distribution that is dominated by direct excitation. The vibrational distribution that follows from the latter depends on the vibrational temperature T_{vib} of the N₂ X state. This is indicated in the figure by the expansion of the coloured lines in the range of 100–10 000 K in steps of 1000 K. The values for $T_{\text{vib}}=1000$ K are highlighted in black, and are close to those for $T_{\text{vib}}=100$ K.

Although about half of the ions are produced in the A and B states, they immediately radiate into the X state so that at any given time nearly all the ions lie in the X state, from which resonance absorption takes place. The fraction $p_{v'}$ of A and B state vibrational level populations with respect to the total N₂⁺ concentration can be found from the relation

$$p_{v'} = \frac{n_{v'(A,B)}}{\sum_{v',v''} n_{v',v''}} \quad (10)$$

Figure 4 describes how this fraction varies with ion lifetime. As expected, at steady state and at longer ion lifetimes the density builds up in the X state so that only a very small fraction of the total density is maintained in the A and B states via direct excitation. At long ion lifetimes the B state contributes only a fraction of 10^{-6} and the A state a fraction of 10^{-4} to the total ion content.

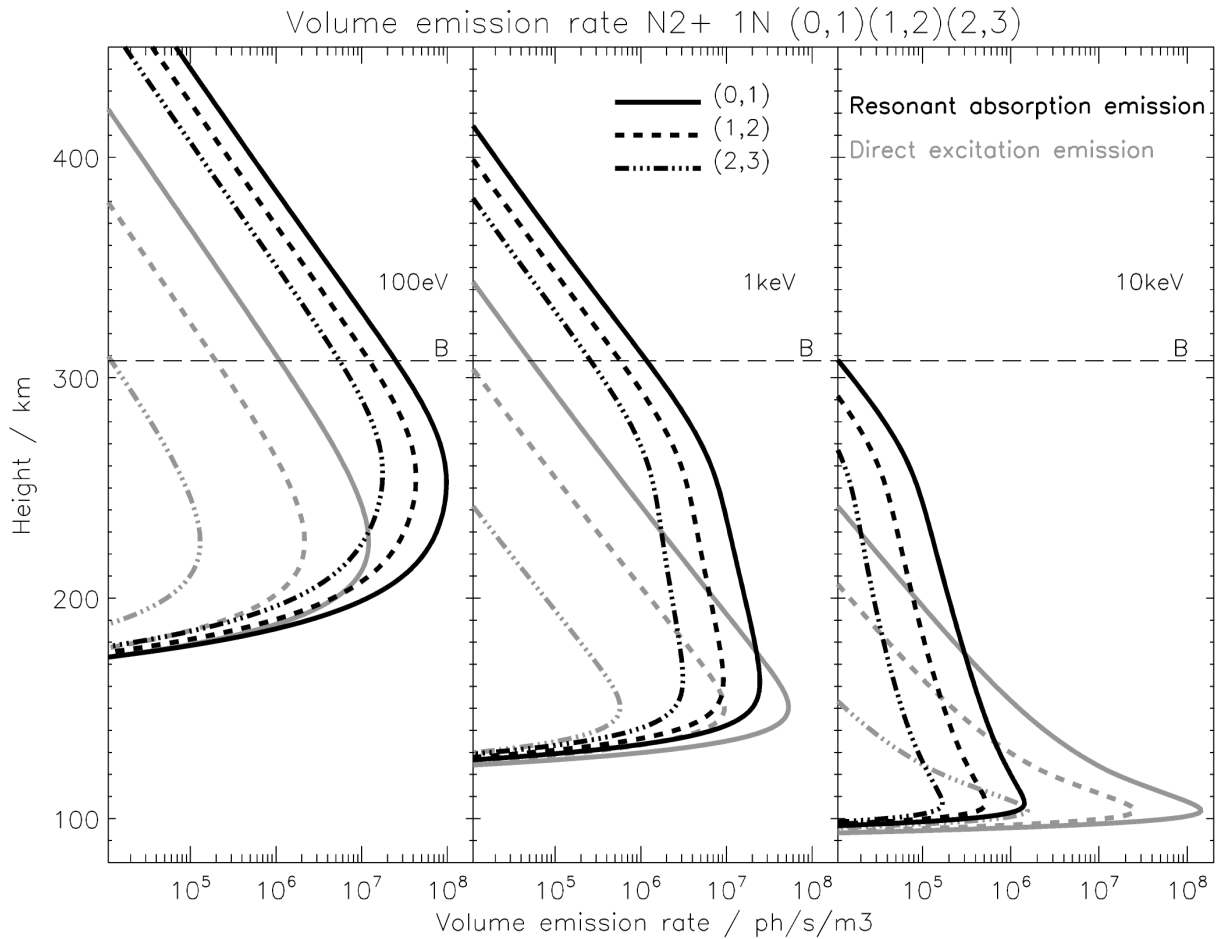


Fig. 6. Synthetic volume emission rates of N₂⁺ (0,1) (solid), (1,2) (dashed) and (2,3) (dot-dash) corresponding to input energies of 100 eV, 1 keV and 10 keV for 30 s. Emission rates from direct excitation are in grey and resonance scattered emissions are in black. The steady state boundary for this condition is drawn at height B.

$$\begin{aligned}
 & \sum_{v'''} \varepsilon(A) q_{(v''' \rightarrow v')} \eta_{N_2^+}^d \\
 & + \sum_{v''} \pi F_{v'' \rightarrow v'} f_{v'' \rightarrow v'} \frac{\pi e^2}{m_e c} \frac{1}{4\pi \epsilon_0} \frac{\lambda^2}{c} n_{v''} \\
 & = \sum_{v''} A_{v' \rightarrow v''} n_{v''} + \frac{n_{v'}}{\tau}
 \end{aligned} \tag{11}$$

$$\begin{aligned}
 & \sum_{v'''} \varepsilon(B) q_{(v''' \rightarrow v')} \eta_{N_2^+}^d \\
 & + \sum_{v''} \pi F_{v'' \rightarrow v'} f_{v'' \rightarrow v'} \frac{\pi e^2}{m_e c} \frac{1}{4\pi \epsilon_0} \frac{\lambda^2}{c} n_{v''} \\
 & = \sum_{v''} A_{v' \rightarrow v''} n_{v''} + \frac{n_{v'}}{\tau}
 \end{aligned} \tag{12}$$

$$\begin{aligned}
 & \sum_{v'''} \varepsilon(X) q_{(v''' \rightarrow v'')} \eta_{N_2^+}^d + \sum_{v'} A_{v' \rightarrow v''} n_{v'} \\
 & = \sum_{v'} \pi F_{v' \rightarrow v''} f_{v' \rightarrow v''} \frac{\pi e^2}{m_e c} \frac{1}{4\pi \epsilon_0} \frac{\lambda^2}{c} n_{v''} + \frac{n_{v''}}{\tau}
 \end{aligned} \tag{13}$$

3.5 Volume emission rates

Following from Eq. (3) the volume emission rate from vibrational level v' in the A or B state to vibrational level v'' in the X state from direct electron impact excitation is given by

$$I_{v' \rightarrow v''}^d = \sum_{v'''} \eta_{v'' \rightarrow v'''}^d b_{v' \rightarrow v''} \text{ [ph/m}^3\text{/s]} \tag{14}$$

The production rate $\eta_{v'' \rightarrow v'''}^d$ is summed over the N₂ X state levels. However, this has an insignificant effect for $T_{\text{vib}} < 1000$ K as the great majority of ions lie on the zeroth vibrational level.

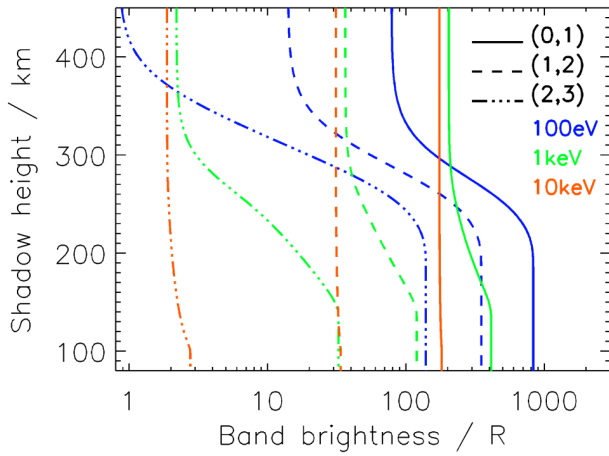


Fig. 7. Band brightness as a function of shadow height for primary electron energies of 100 eV (blue), 1 keV (green) and 10 keV (red) for the N_2^+ bands (0,1) (solid line), (1,2) (dashed) and (2,3) (dot-dash).

Using Eq. (4) the volume emission rate from vibrational level v' in the A or B state to vibrational level v'' in the X state due to resonance absorption of solar photons is given by

$$I_{v' \rightarrow v''}^s = \left(\sum_{v''^*} \eta_{v''^* \rightarrow v'}^s \right) b_{v' \rightarrow v''} \quad [\text{ph}/\text{m}^3/\text{s}] \quad (15)$$

where the summation in this case is over all vibrational levels v''^* of the N_2^+ X state. The production rate $\eta_{v''^* \rightarrow v'}^s$ strongly depends on the distribution of vibrational levels in the N_2^+ X state and consequently greatly affects the vibrational distribution in the excited states. The total emission rate is given by

$$I_{v' \rightarrow v''}^{\text{total}} = n_{N_2^+} p_{v'} A_{v' \rightarrow v''} \quad [\text{ph}/\text{m}^3/\text{s}] \quad (16)$$

where $n_{N_2^+}$ is the total ion density.

The ion chemistry model is run for a constant energy flux of $1 \text{ mW}/\text{m}^2$ and for different monoenergetic electron energy distributions in the range 100 eV to 10 keV to calculate the ion production rate and density of N_2^+ as a function of time and height. Figure 5 shows the ion lifetime resulting from the ion chemistry model using input from MSIS atmospheric model for a typical atmosphere at 07:00 UT in January over Svalbard with A_p index of 7 and solar radio flux f107av of 77.

Volume emission rate profiles were obtained for direct excitation of 30 s to reach steady state at heights up to 300 km using Eq. (14), and for resonance scattered emissions with a sunlit ionosphere, using Eq. (15). The resulting profiles are shown in Fig. 6 for three monoenergetic primary electron spectra of 100 eV, 1 keV and 10 keV. The bands of interest are N_2^+ 1N (0,1), (1,2) and (2,3) plotted with solid line, dashes and dot-dash respectively. Resonance scattered

emission is drawn in black and direct excitation emission in grey. It is evident from these results that the photon scattering contribution becomes increasingly significant at energies below 1 keV. The height labelled B represents the steady state boundary.

In order to compare the modelled emissions with those measured, we now consider how the modelled total brightness in each of the three bands of interest varies with shadow height. In Fig. 7 the total brightness is plotted for three primary electron input energies. It can be seen that the enhancement from resonance scattering increases with decreasing energy. For example, for electron energies of 100 eV (blue curves) at steady state, the brightness of the (2,3) band increases by two orders of magnitude as the shadow height decreases from 400 km to 250 km. The effect is similar for the (1,2) band, but to a lesser extent; for the (0,1) band the brightness increases by an order of magnitude. For higher energies (green and red curves) the increase in brightness with decreasing shadow height is less pronounced, being almost negligible for energies of 10 keV, due to the short ion lifetime at these heights.

The total brightness ratios (2,3)/(0,1) and (1,2)/(0,1) are plotted in Fig. 8 as a function of shadow height and using a range of input energies, and for T_{vib} of 1000 K. The ratio resulting from direct excitation is independent of energy, and is 0.01 for (2,3)/(0,1) and 0.18 for (1,2)/(0,1). With the inclusion of resonance scattering the ratios become a function of energy, increasing with decreasing electron energy. For energies below 100 eV the brightness ratio of (2,3)/(0,1) ratio is greater than 0.17, and the (1,2)/(0,1) is greater than 0.42.

The contribution of resonance scattering to observed height integrated N_2^+ 1N emissions depends on shadow height, electron energy and the band in question. Figure 9 shows the enhancement of total brightness compared to that resulting from only direct excitation for the three bands of interest. Two effects are noticeable. Firstly, the resonance absorption enhancement increases with the vibrational v' level. Secondly, the maximum enhancement is reached when the shadow height is below the height of peak ion density. For low energies the enhancement starts at higher altitudes and also reaches a maximum at higher altitudes.

3.6 g-values

Scattering has been characterised by the g-value (Chamberlain, 1961), which is defined as the number of photons scattered per second per unit atom if there were no deactivation. In the present work the g-value should characterise resonance scattering per molecular N_2^+ ion. A problem lies in that different vibrational levels of N_2^+ X have different resonant absorption efficiencies. These efficiencies are presented in Table 4 for the 1N band system. Furthermore, the vibrational distribution in the N_2^+ X levels depends on the initial distribution from direct excitation and the re-distribution by resonance absorption, which is a function of ion lifetime. Hence,

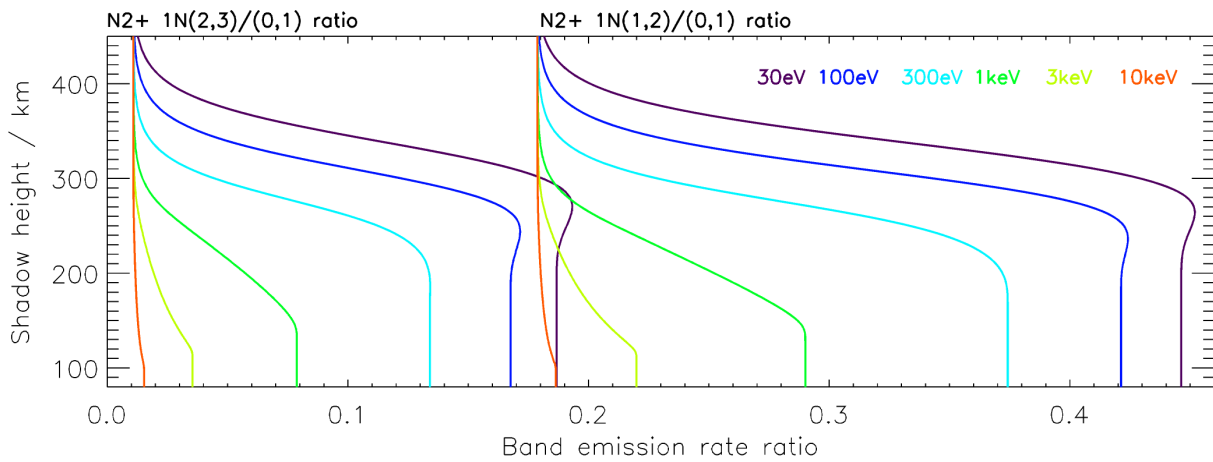


Fig. 8. Band brightness ratios as a function of shadow height for different primary electron energies for N₂⁺ 1N (2,3)/(0,1) (left) and (1,2)/(0,1) (right).

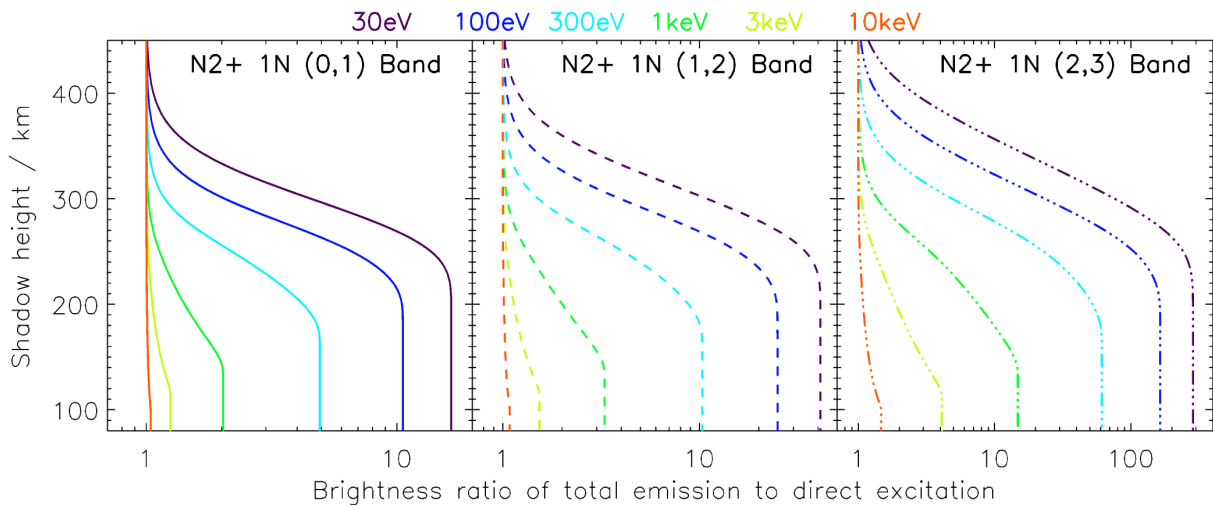


Fig. 9. The brightness of N₂⁺ 1N (0,1), (1,2) and (2,3) bands with respect to the brightness of the same bands from direct excitation for a range of input electron energies.

it is possible to quantify a g-value for a particular vibrational level for a specific height, but it is impossible to assign a single g-value for the total N₂⁺ population.

3.7 Rotational temperatures

As detailed in Jokiahho et al. (2008), rotational temperatures of the N₂⁺ 1N bands are related to the temperature of the parent neutral population. As this temperature is strongly height dependent, it can be used to assess the energy of the electrons creating auroral emissions. In sunlit aurora the rotational temperatures estimated from the height-integrated spectra will be enhanced for two reasons. Firstly, resonance scattering produces the strongest enhancement in the aurora at

Table 4. N₂⁺ X resonance absorption efficiencies to N₂⁺ B in units of [ph/s] per ion in the X state.

N ₂ ⁺ 1N	v′=0	v′=1	v′=2	v′=3
v″ * =0	8.240e-2	1.995e-2	2.538e-3	5.289e-5
v″ * =1	6.079e-2	2.219e-2	3.246e-2	5.707e-3
v″ * =2	2.564e-2	6.650e-2	4.716e-3	3.183e-2
v″ * =3	7.389e-3	4.793e-2	5.300e-2	1.827e-4
v″ * =4	2.032e-3	1.874e-2	5.855e-2	3.790e-2
v″ * =5	—	6.711e-3	3.188e-2	5.589e-2

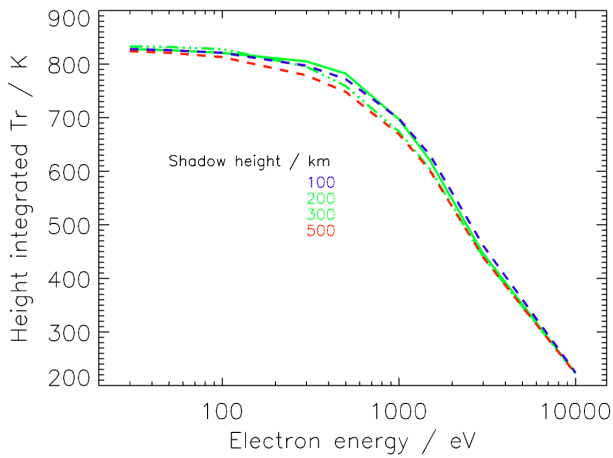


Fig. 10. Height integrated rotational temperature profiles as a function of primary electron energy and shadow height.

the highest altitudes, where the neutral temperature is greatest. Secondly, after multiple scattering, the rotational temperature will tend to the spectral temperature of the solar spectrum as it is in a collisionless environment. Complete modelling of the distribution of rotational intensities is outside the scope of this paper, but the lowest limit to an estimated rotational temperature can be obtained by assuming that the N_2^+ population retains the rotational distribution of the parent N_2 population (i.e. without taking account of redistribution in resonance scattering). In Fig. 10 this variation of rotational temperature with shadow height and input energy has been estimated using the theoretical model results. A synthetic spectrum is obtained from the model emission rate profiles for different input energies. These spectra are integrated in height and fitted over the same wavelength range as the observations to find the rotational temperature. The effect on the rotational temperature of different shadow heights is shown in colour.

4 Experimental results

An overview of the data used in this study is shown in two different representations in Fig. 11. In Fig. 11a the data are plotted against local time in day after 1 January 2007. In Fig. 11b the same data points are ordered with hours UT. In each part the data are presented in four panels: three ratios N_2^+ 1N (1,2)/(0,1), N_2^+ 1N (2,3)/(0,1), N_2 2P (0,3)/ N_2^+ 1N (0,1) and rotational temperature. All the data in this section are ordered by shadow height using colour coding.

From the first set of figures in Fig. 11a it can be seen that the values for the 1N ratio (1,2)/(0,1) in the top panel are in the range 0.1–0.4 and those for the 1N ratio (2,3)/(0,1) are in the range 0.01–0.3. These values can be compared with the theoretical values of Fig. 8, and are in good agreement.

The lower range in both cases is somewhat higher than the theoretical values, but this may be accounted for by the value of vibrational temperature being too high at 1000 K for auroral heights. The ratio of N_2 to N_2^+ emissions in the third panel is inversely proportional to the enhancement of the ion emission in resonance scattering. As we do not model the 2P bands, only relative variations are of interest. The fourth panel shows clearly that the rotational temperatures are enhanced for low shadow heights. The 1N ratios also increase with decreasing shadow height.

In Fig. 11b the effect of local time is apparent immediately, with two distinct populations seen in all four panels. Most of the data with shadow height below 250 km occur between 04:00–10:00 UT when Svalbard is under the morning oval and in the cusp. The 1N ratios in the two top panels demonstrate an increasing ratio with decreasing shadow height, which follows the increase of UT. In the third panel it is noticeable that the ratios of N_2 to N_2^+ emissions are much lower in the morning hours than the evening, indicating the effect of increased emission from scattering. The rotational temperatures are clearly higher during the morning hours, as seen in the bottom panel, and again there is some indication of ordering with shadow height. The population from the evening aurora between 18:00–23:00 UT is when the statistical oval is overhead on Svalbard. The 1N ratios are lower, and the rotational temperatures are lower, corresponding to both high shadow heights and more energetic precipitation.

In order to study these separate populations in more detail, the data have been ordered with band brightness in Fig. 12, using the same format for the ratios and rotational temperature, and using colour to display the shadow height. The data on the left are from 03:00–11:00 UT and those on the right are from 19:00–01:00 UT. During the evening and night hours the ratio of 1N (1,2)/(0,1) in the top panel of Fig. 12b decreases as the brightness increases, which is the possible effect of increasing energy with increasing brightness. The second panel of Fig. 12b is more noisy, so no trend is seen. In both these panels there are some higher values of ratios associated with lower shadow heights. The third panel of Fig. 12b is as expected for the ratio of the neutral N_2 to N_2^+ . The constant proportionality is seen, with little effect from sunlight. The spread of data points reduces with increased brightness, with the data converging on the constant value of about 0.04. In the bottom panel of Fig. 12b there is a trend to lower rotational temperatures with increasing brightness, again indicating a relationship between energy and brightness.

The morning and cusp hours shown in Fig. 12a are very different from the evening hours. The enhanced ratios are clearly organised by shadow height in the top two panels. There is a distinct group of data points associated with a shadow height of >400 km with low ratios and high brightness, which follow the nightside distribution. For these data the aurora is dominating the resulting ratio values. In the third row of panels the scatter in the ratio of N_2 to N_2^+ is

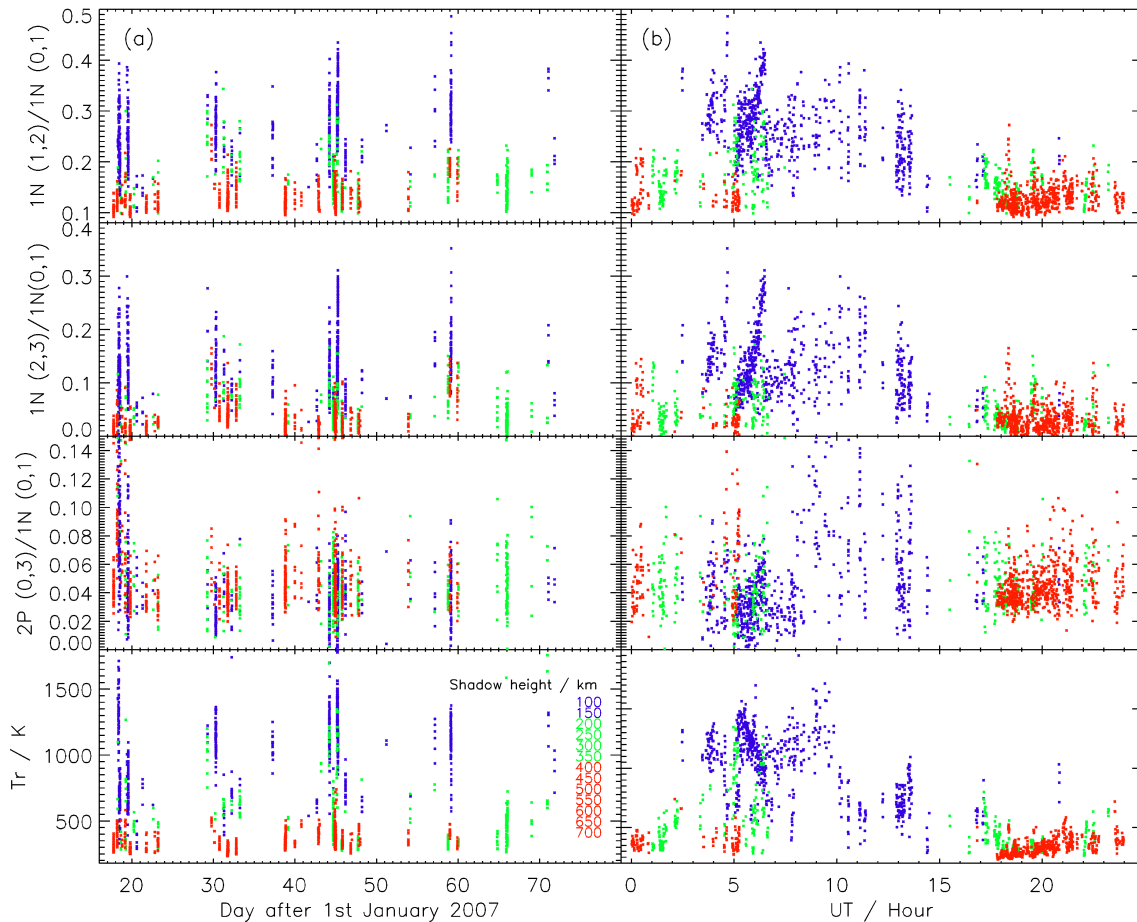


Fig. 11. (a) Ratios of N_2^+ 1N (1,2)/(0,1), (2,3)/(0,1), N_2 2P (0,3)/1N (0,1) and rotational temperature as a function of number of days since 1 January 2007. Solar shadow height (excluding screening height) is shown in colour. (b) Ratios of N_2^+ 1N (1,2)/(0,1), (2,3)/(0,1), N_2 2P (0,3)/1N (0,1) and rotational temperature as a function of universal time. Solar shadow height (excluding screening height) is shown in colour.

greater for the morning hours than for the evening hours. In both cases the high ratios are a result of the larger experimental uncertainty for lower brightnesses. However, it is significant that there is a range of ratios below the constant value of approximately 0.04 seen on the night side. Ratios as low as 0.01 are seen. These values indicate an enhancement of N_2^+ which can be estimated from the theoretical values in Fig. 9 for N_2^+ 1N (0,1) as a four-fold increase. Our steady state assumption allows us to estimate the characteristic electron energy required to produce the enhancement assuming the shadow height is known; e.g. for shadow heights of 200 km and 300 km such ratios were found to correspond to electron energies of 300 eV and 30 eV, respectively. The bottom panel of Fig. 12a shows two groups of data points for rotational temperature versus brightness during the morning and cusp hours: one low energy, high temperature (low shadow heights) and another higher energy, lower temperature (high shadow heights).

Finally the 1N ratios (1,2)/(0,1) have been plotted versus rotational temperature in Fig. 13 for the morning hours 03:00–10:00 UT. The high temperatures up to 1500 K are found for low shadow heights and high ratios. The minimum temperatures estimated in Fig. 10 from our simple model are below 1000 K for all energies and shadow heights, so there is a strong effect from scattering which requires more careful analysis. Such high temperatures suggest considerable redistribution between the rotational states.

5 Discussion and conclusions

The aim of the present work is to assess and quantify the effects of resonance scattering on N_2^+ 1N emissions at high latitudes. The theoretical treatment of Sect. 3 solves the balance equations for steady state to give the populations of all the vibrational levels of the N_2^+ X, A and B states, and hence, using an ion chemistry model, the emissions from direct excitation

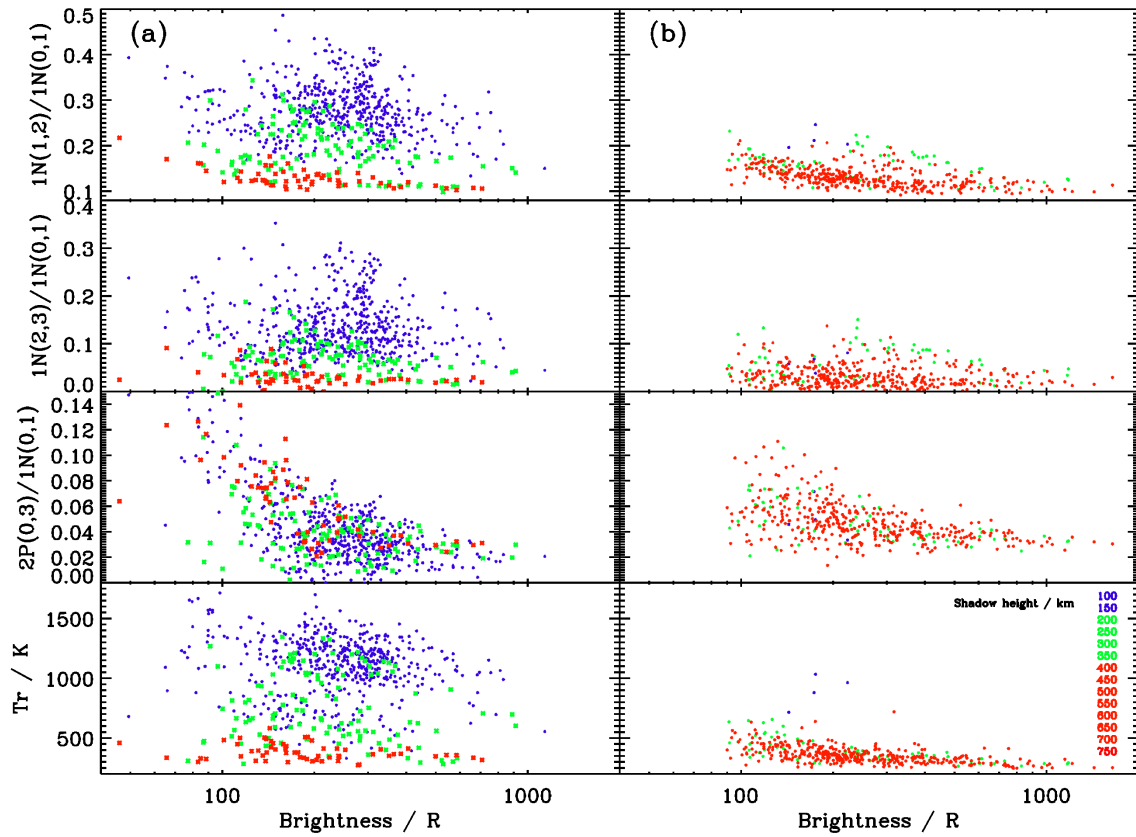


Fig. 12. Ratios of N₂⁺ 1N (1,2)/(0,1), (2,3)/(0,1), N₂ 2P (0,3)/1N (0,1) and rotational temperature as a function of N₂⁺ 1N (0,1) band brightness for (a) morning-day time and (b) evening-night time spectra. Solar shadow height (excluding screening height) is shown in colour.

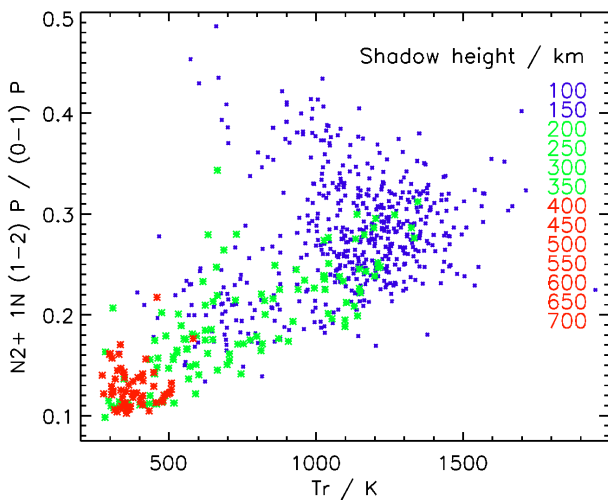


Fig. 13. The ratio of N₂⁺ 1N (1,2)/(0,1) as a function of rotational temperature and shadow height (excluding screening height) for 03:00–10:00 UT.

and from scattering, with changing shadow height. The main result of this work shows that for shadow heights above about 400 km the 1N bands and their ratios are almost unaffected, but for shadow heights below 150 km (i.e. fully illuminated) there are significant enhancements which increase with decreasing energy. At very low energies of 100 eV the increase in brightness is found to be a factor of 10 (Fig. 7).

The variation in the ratios of the 1N bands have been modelled for (1,2)/(0,1) and (2,3)/(0,1) for several input energies, and as a function of shadow height, in order to compare with the observations from more than two winter months. The observed ratios have a lower limit than the theoretical values, which can be explained by the choice of T_{vib} in the modelling. We have chosen a vibrational temperature of 1000 K as a conservative estimate. It can be determined from Fig. 4 that the ratios will decrease with a smaller value of T_{vib} as seen in the relative populations shown in Fig. 3. The non-sunlit N₂⁺ 1N (1,2)/(0,1) ratio was measured by Vallance Jones (1974) as 0.1290, and the (2,3)/(0,1) ratio as 0.0017. These values are both smaller than our theoretical ratios, but in the range that we observe.

The main result of the present work is that the ratios of the 1N bands are a function of energy under sunlit conditions.

The observations in this statistical study do not give an independent estimate of electron precipitation. The results from previous observations of the magnitude of the effect of resonance scattering make claims of specific percentages. It is clear from the present work that such numbers as 56% quoted by other observers are not valid without knowledge of the energy spectrum of the precipitation that has excited and ionised the nitrogen molecules. Over the two months of 24 h of twilight and solar illumination that we have measured, the emissions are clearly from a large range of energies, i.e. from precipitation events that vary significantly.

In order to determine the effect of resonance scattering more accurately it is necessary to know the energy of precipitation, which indicates that a case by case approach is more suitable. With the advantage of incoherent scatter radar to provide electron density profiles, the incoming energies can be inferred. Jokiahho et al. (2008) have used the EISCAT radar to compare energies derived from electron densities and modelling with those derived from optical measurements of N_2^+ using rotational temperatures. It was this study that gave impetus to the need to determine the effects of sunlight on these important emissions. There are clear events within the present observations that will be used for future case studies. One event can be readily distinguished in the overview plots of Fig. 11 between 05:00 UT and 06:30 UT. This was a period of continuous electron precipitation on 14 February 2007. During this time the ratios of N_2^+ (1,2)/(0,1) and (2,3)/(0,1) were steadily increasing whilst the rotational temperature was steadily decreasing as a function of time, indicating increasing electron energy.

We have established in the observations that the rotational temperature is strongly affected by the resonance scattering, not only through the peak in the emission profile shifting to higher altitude with higher corresponding neutral temperatures. Values of T_{rot} in excess of 1000 K suggest considerable redistribution between the rotational states. In order to calculate the full effect, a complete model is required which includes all rotational states, radiative and collisional processes (including inelastic collisions with N_2 and electrons). This is outside the scope of this paper, but is important for future work. It should be noted however, that if inelastic collisions not leading to the loss of N_2^+ ions are important, their effect will be to equalise the rotational temperatures of N_2^+ and the neutrals or electrons. These temperatures are typically below 1000 K for the conditions presented, so any observation of T_{rot} in excess of this must come from heights where collision frequencies are negligible compared to characteristic frequencies of resonance scattering (g-factors). The fact that such values of T_{rot} are indeed observed may point to the importance of ion upflow processes.

This study also suggests two directions for further work. One is a comparison of “cusp” observations with shadow heights over 400 km, and those with shadow heights of 100 km, especially if there are corresponding radar data. The

other is a time dependent study of the effects of scattering. When the lifetime of the N_2^+ ion becomes comparable with the scattering timescale, and with timescales of temporal variations in the aurora, the steady state solution poorly describes the reality. An interesting implication is that the sun-illuminated N_2^+ population at high altitudes serves as a “marker” of the F-region plasma, in a way similar to the metastable O^+ population, opening the possibility for direct optical observations of plasma flows (Dahlgren et al., 2009).

Acknowledgements. N. Ivchenko was supported by the Swedish Research Council. D. Lummerzheim provided much valuable insight into the science, and the modelling. The HiTIES instrument is operated by the University of Southampton, funded by the PPARC of UK and is a collaboration between University College London and Boston University. The author would like to thank M. Wedlund for help in operating HiTIES during the campaign, J. Holmes and M. Dyrlund (UniS) for all the logistical help given at Svalbard. Appreciation for the data collection and analysis tools goes to D. Whiter, J. Sullivan and H. Dahlgren.

Topical Editor M. Pinnock thanks two anonymous referees for their help in evaluating this paper.

References

- Bates, D. R.: The emission of the negative system of nitrogen from the upper atmosphere and the significance of the twilight flash in the theory of the ionosphere, *Proc. R. Soc.*, A196, 562–591, 1949.
- Broadfoot, A. L.: Resonance Scattering by N_2^+ , *Planet. Space Sci.*, 15, 1801–1815, 1967.
- Chakrabarti, S., Pallamraju, D., Baumgardner, J., and Vaillancourt, J.: HiTIES: A High Throughput Imaging Echelle Spectrograph for ground-based visible airglow and auroral studies, *J. Geophys. Res.*, 106, 30337–30348, 2001.
- Chamberlain, J. W.: *Physics of the aurora and airglow*, Academic Press, p. 424, 1961.
- Dahlgren, H., Ivchenko N., Lanchester, B., Ashrafi, M., Whiter, D., Marklund, G., and Sullivan, J.: First direct optical observations of plasma flows in the metastable O^+ ion in discrete aurora, *J. Atmos. Sol. Terr. Phys.*, 71, 228–238, 2009.
- Degen, V.: Vibrational Enhancement and the Excitation of N_2^+ and the First Negative System in the High-Altitude Red Aurora and the Dayside Cusp, *J. Geophys. Res.*, 86(A13), 11372–11378, 1981.
- Degen, V.: Modeling of the N_2^+ First Negative Bands in the Sunlit Aurora, *Planet. Space Sci.*, 35(8), 1061–1066, 1987.
- Galand, M., Baumgardner, J., Pallamraju, D., Chakrabarti, S., Løvhaug, U. P., Lummerzheim, D., Lanchester, B. S., and Rees, M. H.: Spectral imaging of proton aurora and twilight at Tromsø, Norway, *J. Geophys. Res.*, 109(A7), A07305, doi:10.1029/2003JA010033, 2004.
- Gattinger, R. L., Vallance Jones, A., Hecht, J. H., Strickland, D. J., and Kelly, J.: Comparison of ground-based optical observations of N_2 second positive to N_2^+ first negative emission ratios with electron precipitation energies inferred from the Sondre Stromfjord radar, *J. Geophys. Res.*, 14(96), 11341–11351, 1991.

- Gilmore F. R., Laher, R. R., and Espy, P. J.: Franck-Condon Factors, R-centroids, Electronic Transition Moments and Einstein Coefficients for Many Nitrogen and Oxygen Band Systems, *J. Phys. Chem. Ref. Data*, 21(5), 1005–1107, 1992.
- Hunten D. M., Koenig, H. J., and Vallance Jones, A.: Rotational Structure of the 3914 Å N_2 Band in Sunlit Aurorae, *Nature*, 183, 453–454, 1959.
- Hunten, D. M.: Sunlit Aurora and the N_2^+ ion: a Personal Perspective, *Planet. Space Sci.*, 51, 887–890, 2003.
- Jokiahho, O., Lanchester, B. S., Ivchenko, N., Daniell, G. J., Miller, L. C. H., and Lummerzheim, D.: Rotational temperature of N_2^+ (0,2) ions from spectrographic measurements used to infer the energy of precipitation in different auroral forms and compared with radar measurements, *Ann. Geophys.*, 26, 853–866, 2008, <http://www.ann-geophys.net/26/853/2008/>.
- Lanchester, B. S. and Rees, M. H.: Field-aligned current reversals and fine structure in a dayside auroral arc, *Planet. Space Sci.*, 35(6), 759–768, 1987.
- Lanchester, B. S., Rees, M. H., Robertson, S. C., Lummerzheim, D., Galand, M., Mendillo, M., Baumgardner, J., Furniss, I., and Aylward, A. D.: Proton and electron precipitation over Svalbard – first results from a new Imaging Spectrograph (HiTIES), *Proc. 28th Ann. Europ. Meeting of Atmospheric Studies by Optical Methods*, S.G.O. Publications, 92, 33–36, 2003.
- Lofthus, A. and Krupenie, P. H.: The spectrum of molecular nitrogen, *J. Phys. Chem. Ref. data*, 6(1), 113–307, 1977.
- Remick, K. J., Smith, R. W., and Lummerzheim, D.: The significance of resonant scatter in the measurement of N_2^+ first negative 0–1 emissions during auroral activity, *J. Atmos. Sol. Terr. Phys.*, 63, 295–308, 2001.
- Romick, G. J., Yee, J.-H., Morgan, M. F., Morrison, D., Paxton, L. J., and Meng, C.-I.: Polar Cap Optical Observations of Topside (>900km) Molecular Nitrogen Ions, *Geophys. Res. Lett.*, 26(7), 1003–1006, 1999.
- Störmer, C.: *The Polar Aurora*, Clarendon Press, 1955.
- Vallance Jones, A. and Hunten, D. M.: Rotational and Vibrational Intensity Distribution of the First Negative N_2^+ Bands in Sunlit Auroral Rays, *Can. J. Phys.*, 38, 458–475, 1960.
- Vallance Jones, A.: *Aurora*, D. Reidel Publishing Company, Dordrecht, Holland, 1974.